

Cationic Conjugated Polymers with Enhanced Doped-State Planarity for *n*-Type Organic Thermoelectrics

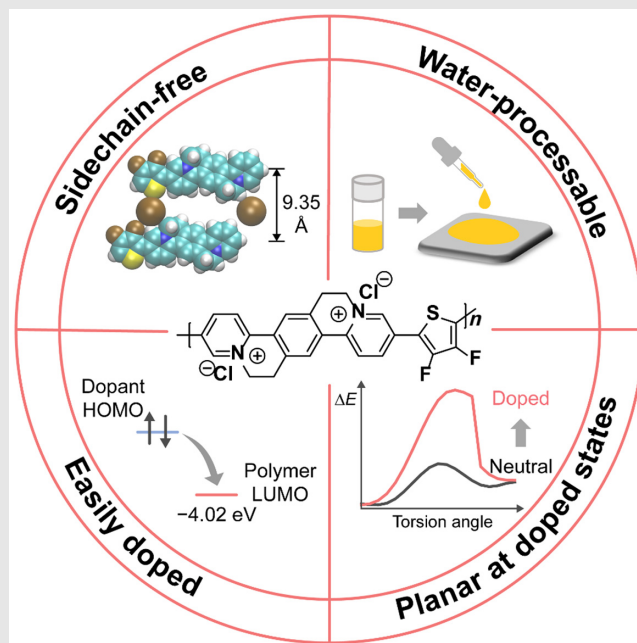
Jiu-Long Li^{1,2†}, Xin-Yu Deng^{1†}, Jupeng Chen¹, Peng-Xiang Fu³, Shuang-Yan Tian¹, Yunfei Wang⁴, Xiaodan Gu⁴, and Ting Lei^{1*}

¹Key Laboratory of Polymer Chemistry and Physics of Ministry of Education, School of Materials Science and Engineering, Peking University, Beijing 100871, ²Luoyang Ship Material Research Institute, Xiamen 361101, ³Beijing National Laboratory of Molecular Science, Beijing Key Laboratory of Magnetoelectric Materials and Devices, College of Chemistry and Molecular Engineering, Peking University, Beijing 100871, ⁴School of Polymer Science and Engineering, Center for Optoelectronic Materials and Devices, University of Southern Mississippi, Hattiesburg, MS 39406

*Corresponding author: tinglei@pku.edu.cn; [†]J.-L. Li and X.-Y. Deng contributed equally to this work.

Cite this: CCS Chem. 2024, Just Published. DOI: 10.31635/ccschem.024.202404274

To date, extensive efforts have been devoted to designing new conjugated polymers with long alkyl or ethylene glycol sidechains. However, these sidechains are insulators, limiting further performance enhancement in doped conjugated polymers. Moreover, the most widely used chlorinated solvents are toxic, limiting the practical applications of many conjugated polymers. Here, we report a water/alcohol processable *n*-type conjugated polymer P(Py2FT), featuring side chain-free cationic backbones. P(Py2FT) exhibits a high *n*-type electrical conductivity of up to 28.1 S cm^{-1} and a high thermoelectric power factor of up to $28.7 \mu\text{W m}^{-1} \text{ K}^{-2}$, comparable to some conventional *n*-type conjugated polymers reported recently. More importantly, cationic polymers display tight molecular packings and interesting enhanced backbone planarity after *n*-doping, which, we envision, provides a new research direction to address the sidechain issue in conventional conjugated polymers. Our work demonstrates that sidechain-free cationic polymers have great potential for green-solvent-processed heavily doped organic electronics.



Keywords: cationic polymers, organic thermoelectrics, *n*-doping, backbone planarity, charge transport

Introduction

Organic thermoelectrics (OTEs) have attracted increasing interest in recent years due to their low toxicity, light weight, good solution processability, and high mechanical flexibility.¹ To achieve high energy-conversion efficiency, both high-performance complementary *p*-type and *n*-type OTEs are required. To date, *p*-type conjugated polymers have demonstrated excellent conductivities over 1000 S cm⁻¹, together with high power factors (PFs) over 100 $\mu\text{W m}^{-1}\text{K}^{-2}$.²⁻⁴ In contrast, only a few *n*-type conjugated polymers have shown conductivities over 10 S cm⁻¹, with PFs exceeding 10 $\mu\text{W m}^{-1}\text{K}^{-2}$.⁵⁻⁷

Many high-performance *n*-type conjugated polymers are based on conventional polymer designs (Figure 1a).⁸⁻¹¹ These polymers are typically linked by carbon–carbon single bonds, resulting in significant conformational disorder. To lock the backbone rotation, complex structures with specifically designed noncovalent interactions are necessary.^{12,13} To address this issue, double-bond-linked polymers were designed (Figure 1b).¹⁴ While these double bonds contributed to rigid rod-like backbones, the double bonds largely stretched out in doped states, leading to lower rotational barriers, considerable energetic disorder, and poor charge-carrier mobility.¹⁵ Additionally, most of these traditional conjugated polymers require long alkyl or ethylene glycol sidechains to guarantee good solution processability. However, these solubilizing sidechains are insulators, hindering the further enhancement of the thermoelectric performance.¹⁶⁻¹⁹ Thus, sidechain-free polymers such as PBFDO or PBDF were reported, which exhibited impressively high *n*-type electrical conductivities, suggesting that sidechain-free polymer design is a new trend for highly conductive *n*-type polymers.^{20,21} However, controlling the doping

level and further modifying the chemical structure in such kind of intrinsically doped polymer remains challenging. Furthermore, the polymer requires high-boiling-point solvents, such as dimethyl sulfoxide, for processing, which limits its facile processability.

Here, we designed and synthesized a novel cationic conjugated polymer, P(Py2FT), to explore the potential of cationic polymers for OTEs (Figure 1c). Compared to traditional polymers with long sidechains, our cationic polymer displayed a significantly reduced lamellar distance and a comparable π – π stacking distance, promoting more compact molecular packing for efficient charge transport. P(Py2FT) exhibited a high *n*-type electrical conductivity of up to 28.1 S cm⁻¹ and an impressive thermoelectric PF of up to 28.7 $\mu\text{W m}^{-1}\text{K}^{-2}$. In addition, we demonstrated that cationic building blocks strongly increased the electron density of the lowest unoccupied molecular orbital (LUMO) across the linkages. This results in a shorter C–C single bond and, consequently, enhanced backbone planarity after doping. Therefore, introducing cationic building blocks is an effective way to enhance the backbone planarity and thus charge transport performance in doped states.

Experimental Methods

Film preparation and doping

Glass substrates were cleaned by ultrasonication in successive baths of pure water, acetone, and isopropanol, with each bath lasting 5 min, followed by plasma treatment with O₂ for 10 min. Before film fabrication, both P(Py2FT) and P(PyT) were dissolved in a 1:1 mixture of 2,2,2-trifluoroethanol (CF₃CH₂OH) and water at a concentration of 3 g/L and stirred at 65 °C for two hours in a nitrogen atmosphere. Thin films were deposited onto

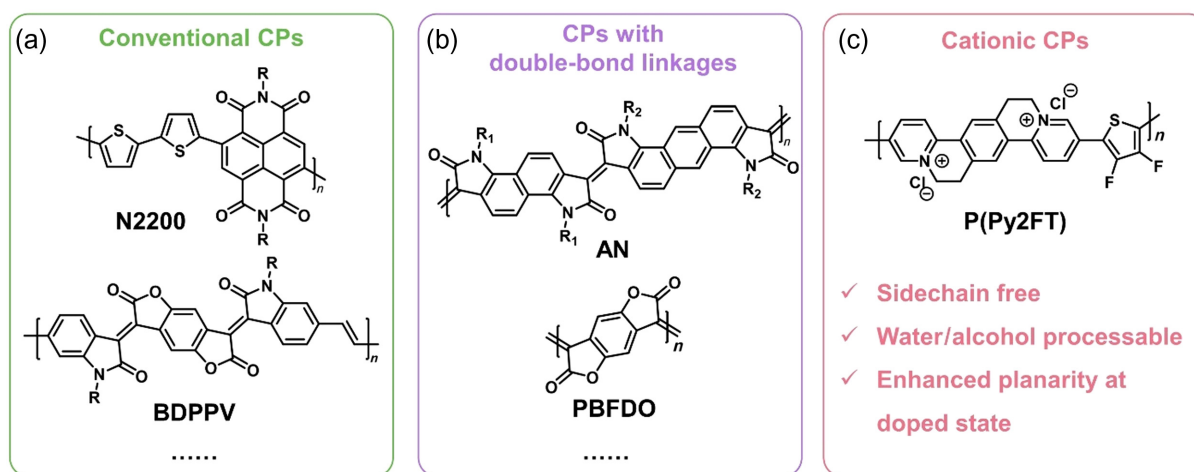


Figure 1 | Chemical structures and features of different types of high-performance *n*-type conjugated polymers (CPs). We categorize these polymers into (a) conventional CPs, (b) CPs with double-bond linkages, and (c) cationic CPs.

glass substrates by spin-coating the polymer solution at 2000 rpm for 60 s. The dopant, tetrakis(dimethylamino)ethylene (TDAE), was purchased from Sigma-Aldrich (Shanghai, China). The polymer films were exposed to TDAE vapor for various times at room temperature within a glove box under the N₂ atmosphere.

Thermoelectric properties measurement

All devices for conductivity and Seebeck coefficient measurement devices were constructed using glass substrates. The conductivities and Seebeck coefficients were collected by four probe measurements within the same N₂ glove box, employing a KeysightB1500A semiconductor parameter analyzer (KEYSIGHT, Colorado Springs, USA). For Seebeck measurement, self-built equipment was used to set the temperature difference. The Seebeck coefficient was calculated by $S = \Delta V_{\text{therm}} / \Delta T$. ΔV_{therm} is the thermal voltage between the hot and cold ends of the device at a temperature gradient ΔT . The ΔV_{therm} was continuously monitored using the Keysight B1500A, and the temperature difference was established by Joule heat (heater) and a circulating water-cooling system. To ensure accuracy, we corrected for the temperature difference ΔT between the two contact pads with two temperature sensing wires (5 nm Cr/20 nm Au bilayer). By tracking changes in the resistance of these temperature-sensing electrodes, the accurate temperature of the contact pads was obtained. The device architecture for Seebeck measurement is shown in [Supporting Information Figure S3](#).

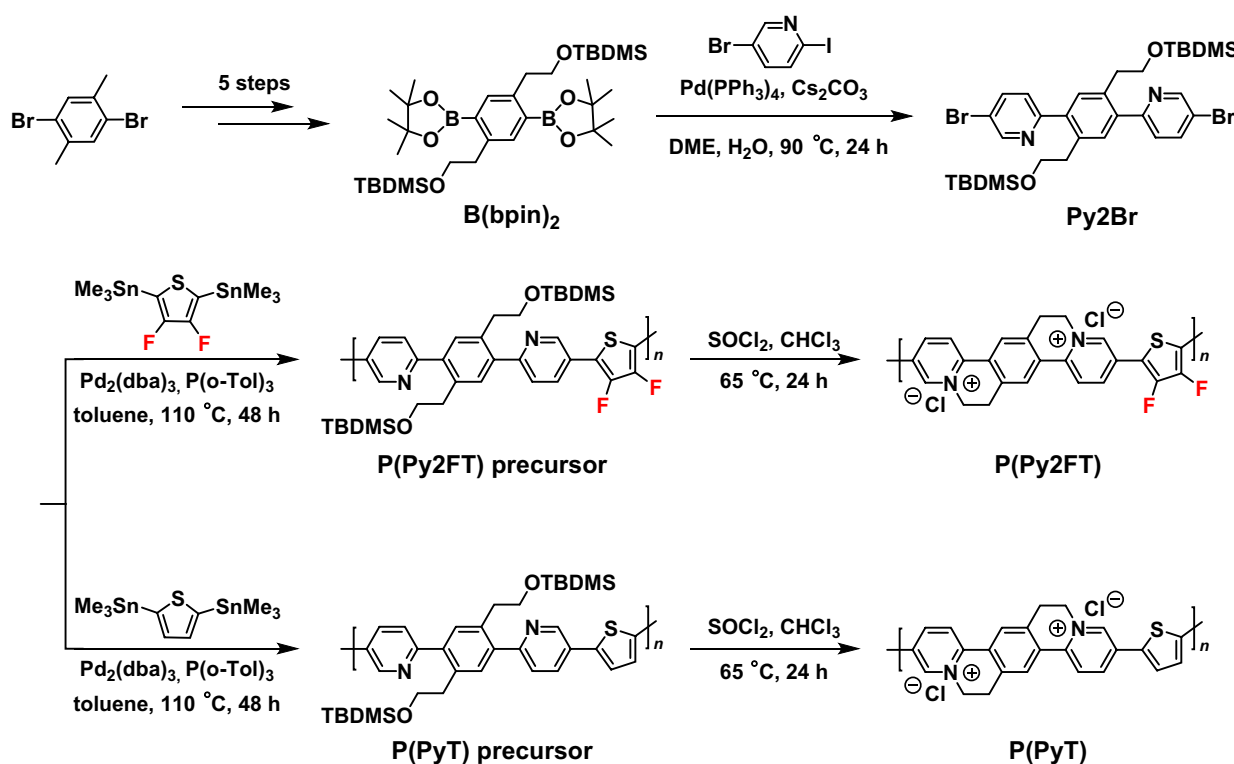
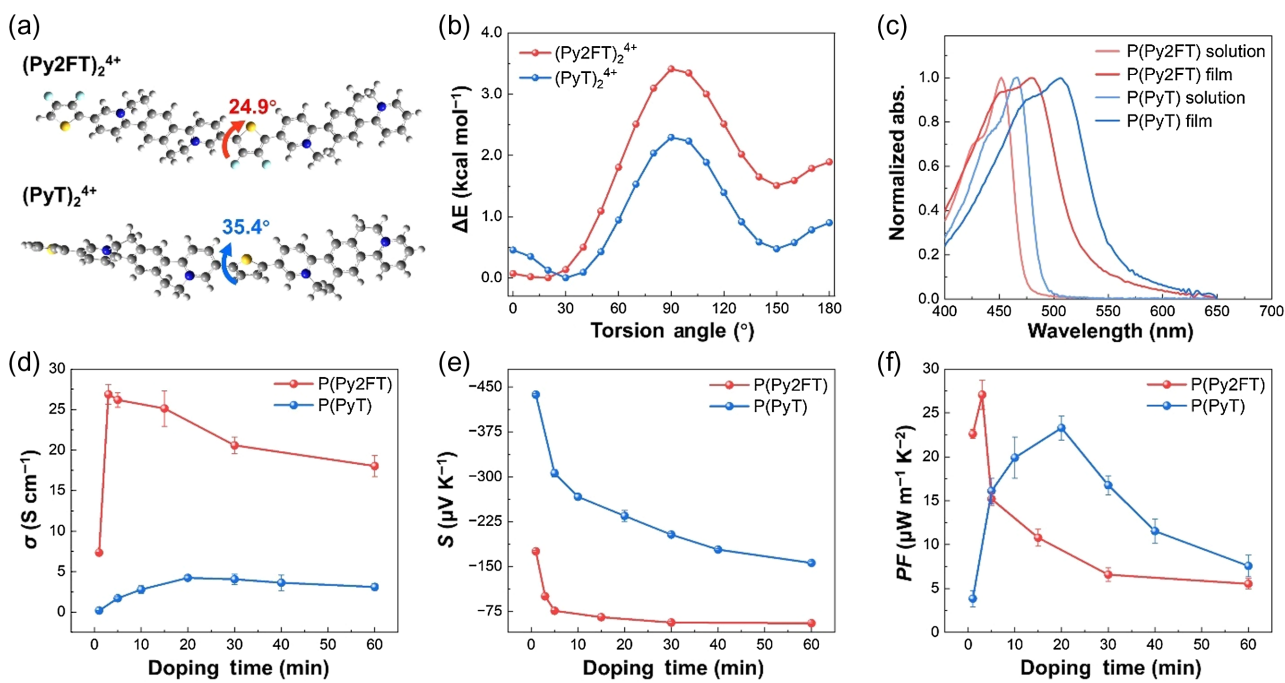
Characterization

Molecular weights were determined by gel permeation chromatography (GPC) on a Waters 1515 instrument (Waters, Milford, USA) at room temperature using chloroform as the eluent. Thermal gravity analyses (TGA) were carried out on a TA Instrument Q600 analyzer (TA Instruments, Shanghai, China). Cyclic voltammetry (CV) measurements were performed on a BASI Epsilon workstation (BASI Corporate Headquarters, West Lafayette, USA). Absorption spectra were recorded on PerkinElmer Lambda 750 UV-vis spectrometer (PerkinElmer, Shelton, USA). Ultraviolet photoemission spectroscopy (UPS) and X-ray photoelectron spectroscopy (XPS) were conducted using a Kratos AXIS Ultra Photoelectron Spectrometer (Kratos Analytical Ltd, Manchester, U.K.) under ultrahigh vacuum conditions (approximately 3×10^{-9} Torr) with an unfiltered He I gas discharge lamp source (21.22 eV) and a monochromatic Al K α source (1486.7 eV, $\theta = 90^\circ$) as the excitation source. Continuous-wave electron paramagnetic resonance (EPR) measurements were conducted on a Bruker Elexsys E580 spectrometer using an ER 4122 SHQE Resonator highly sensitive EPR cavity (Bruker, Massachusetts, USA). The grazing-incidence wide-angle

X-ray scattering (GIWAXS) experiments were performed on a XenocsXucess 2.0 beamline (Xenocs Inc, Holyoke, USA), with an incident X-ray angle of 0.2 deg and wavelength of 1.54 Å. The scattered signals were collected by a Pilatus 1M detector at a sample-to-detector distance of 150 mm. All density functional theory (DFT) calculations were performed using the Gaussian 16 package.²²

Results and Discussion

Conjugated polymers with cationic backbones have been previously reported, known for their low LUMO energy levels that are suitable for *n*-doping.^{23–25} However, these polymers have not received enough attention over the years, particularly in the field of OTE applications. The relationship between their structure and thermoelectric performance remains poorly understood. To delve into the molecular design strategy, we designed and synthesized a new cationic polymer, namely P(Py2FT). For comparison, the previously reported polymer P(PyT) was also synthesized.²⁴ Scheme 1 illustrates the synthetic routes to both cationic polymers. The B(bpin)₂ was synthesized through five synthetic procedures with the initial compound 1,4-dibromo-2,5-dimethylbenzene, following the procedures in previous literature.²⁴ It is worth noting that the previous reaction and polymerization conditions often resulted in more side products, low molecular weight polymers, and incomplete ring closure, leading to notable structural defects and poor device performance. Here, to improve the regioselectivity of the Suzuki coupling reaction, we substituted 2,5-dibromopyridine with 5-bromo-2-iodopyridine to react with B(bpin)₂ to give the critical monomer, Py2Br. In the next polymerization step, we strategically replaced the catalyst Pd(PPh₃)₄ with Pd₂(dba)₃+P(o-Tol)₃, which enhanced the molecular weights ([Supporting Information Section 3](#)). Using the 2,5-bis(trimethylstannyl)-3,4-difluorothiophene (2FT) as the organotin reagent to copolymerize with Py2Br by Stille coupling reaction, the cationic polymer precursor was obtained. The polymer precursor was purified by Soxhlet extraction, and the chloroform portion was collected. Further reacting with SOCl₂ to close the ring under a modified reaction condition, the new cationic polymer, P(Py2FT), can be obtained. The reference polymer P(PyT) was synthesized using a similar route. After modifying the reaction conditions, we obtained defect-free cationic polymers, which benefit the charge-carrier transport and the reproducibility of the device performance. The chemical structures of these synthesized compounds were verified by ¹H NMR and ¹³C NMR spectra ([Supporting Information Figures S25–S35](#)). GPC was used to characterize the molecular weights of the precursor of cationic polymers [P(Py2FT) precursor: Mn = 18.8 kDa, polydispersity index (PDI) = 2.33; P(PyT) precursor: Mn = 17.6 kDa, PDI = 2.67;

**Scheme 1** | Synthetic routes to **P(Py2FT)** and **P(PyT)**.**Figure 2** | (a) DFT-optimized geometries for $(\text{Py2FT})_2^{4+}$ and $(\text{PyT})_2^{4+}$. The number 4 represents four positive charges. (b) Relaxed PES of the torsion angle between two repeating units for $(\text{Py2FT})_2^{4+}$ and $(\text{PyT})_2^{4+}$. DFT calculations were carried out at the B3LYP/6-311G(d,p) level. (c) Normalized UV-vis spectroscopy of cationic polymers in $\text{CF}_3\text{CH}_2\text{OH}$ dilute solutions (solid lines) and thin films (dashed lines). (d) Electrical conductivities (σ), (e) Seebeck coefficient (S), and (f) PF of TDAE doped **P(Py2FT)** and **P(PyT)** with various doping times.

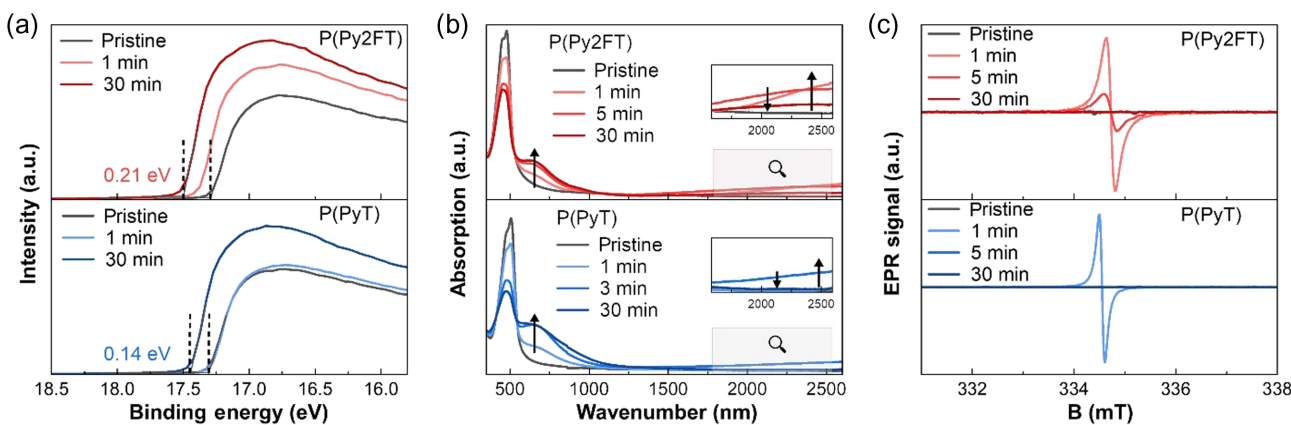


Figure 3 | (a) UPS binding energy, (b) UV-vis-NIR spectra, and (c) continuous wave EPR spectra of both P(Py2FT) (top) and P(PyT) (bottom) films in their pristine and TDAE-doped states. The doping time presents TDAE exposure time.

[Supporting Information Figure S1 and Table S1]. Both cationic polymers showed good thermal stability with decomposition temperatures over 200 °C (Supporting Information Figure S2).

Figure 2a shows the DFT-optimized molecular structures of the cationic backbones. For $(\text{Py2FT})_2^{4+}$, the F···H distances (2.16 Å) are notably smaller than the sum of their van der Waals radii (2.67 Å), indicating the presence of stabilizing intramolecular interactions.^{26,27} Consequently, the introduction of F substituents in $(\text{Py2FT})_2^{4+}$ reduced the torsion angles to 24.9°. In contrast, $(\text{PyT})_2^{4+}$ obviously deviates from planarity by 35.4°. Relaxed potential energy scans (PES) further revealed that $(\text{PyT})_2^{4+}$ had a minimum energy conformation at a torsion angle of approximately 30°, with a modest barrier height of 2.2 kcal/mol (Figure 2b). However, $(\text{Py2FT})_2^{4+}$ exhibited a flat energy surface from 0 to 20°, followed by a steeper and higher torsion barrier. These calculations consistently underscore the finding that P(Py2FT) possesses a more planar and rigid backbone than P(PyT).

Figure 2c depicts the ultraviolet-visible-near-infrared (UV-vis-NIR) absorption spectra of cationic polymers in both dilute solutions and films. In solution, both P(Py2FT) and P(PyT) exhibit similar absorption characteristics, with peak maxima at 452 and 466 nm, respectively. When transitioning to the film state, a notable redshift of absorption was observed for both polymers, suggesting enhanced backbone planarity in the solid state.¹⁷ Moreover, P(Py2FT) exhibited narrower absorption peaks in the film compared to P(PyT), which can be attributed to its reduced conformational disorder.²⁸ CV measurements revealed that introducing electron-withdrawing F substituents in P(Py2FT) reduces its LUMO energy level to 4.02 eV, which is 0.24 eV lower than P(PyT) (Supporting Information Figure S4 and Table S3). This deepening of LUMO is beneficial for efficient *n*-type doping in conjugated polymers.^{29,30} We selected TDAE as

the *n*-dopant, due to its strong reducibility and small molecular size.^{5,31} Unlike conventional conjugated polymers using toxic solvents, both cationic polymers can be processed with water, offering more sustainable, efficient, and low-cost fabrication methods. To optimize their electrical performance, both polymers were dissolved in a 1:1 mixture of water and $\text{CF}_3\text{CH}_2\text{OH}$ (Supporting Information Figures S5-S7). In the pristine state, these cationic polymers exhibited low electrical conductivities, approximately 0.001 S cm^{-1} . Upon TDAE doping, their conductivities increased significantly by three orders of magnitude (Figure 2d). After a 3-minute exposure to TDAE, P(Py2FT) achieved a maximum electrical conductivity of 28.1 S cm^{-1} , six-fold higher than that of P(PyT) (4.70 S cm^{-1}). Further increasing the doping time, the conductivities for both cationic polymers slightly decreased, which might be due to several factors, such as dopant-induced morphology change³² or the formation of defects within the polymer due to doping.³³ The negative Seebeck coefficients suggest an electron-dominated transport in these cationic polymers (Figure 2e). As the doping time increased, the Seebeck coefficient of P(Py2FT) consistently remained lower than that of P(PyT), suggesting that P(Py2FT) may exhibit a higher doping level. Ultimately, the maximum PFs for P(Py2FT) and P(PyT) reached 28.7 and $24.7 \mu\text{W m}^{-1} \text{ K}^{-2}$, respectively (Figure 2f). These values are comparable to some conventional *n*-type conjugated polymers reported recently.^{30,34}

UPS were collected to measure the doping level (Figure 3a). The secondary electron cutoff of P(Py2FT) shifted by 0.21 eV when exposed to TDAE vapor for 30 min, equivalent to an upward movement of its Fermi level by 0.21 eV. This shift was notably larger than that observed in P(PyT) (0.14 eV) under the same doping time. This result indicates a higher doping level in P(Py2FT), which is further supported by XPS

measurement ([Supporting Information Figure S10](#)). Upon doping, the XPS sulfur 2p spectra of P(Py2FT) films exhibited a larger shift to a lower binding energy, which is attributed to the formation of negatively charged polaronic S atoms on the doped polymer backbone. In contrast, this shift in the doped P(PyT) was less pronounced, indicating a lower doping level. The XPS estimated carrier concentration for P(Py2FT) doped for 30 min was $3.06 \times 10^{20} \text{ cm}^{-3}$, which was three times higher than that of P(PyT) ([Supporting Information Figure S11 and Table S1](#)). To monitor the doping process, UV-vis-NIR absorption spectroscopy was employed (Figure 3b). Upon doping, the absorption spectra revealed that the neutral bands of both cationic polymers became bleached along with the emergence of new absorbance peaks at 640 nm and beyond 2000 nm. As the doping level increased, the broad peak beyond 2000 nm decreased and eventually disappeared, while the absorption peak at 640 nm consistently grew. This opposite behavior of these two absorption bands indicates the presence of different types of species during the doping process.³⁵ To further identify these species, EPR spectroscopy was used (Figure 3c). After one minute of TDAE doping, the EPR signatures of both polymers significantly increased, indicating that species at low doping levels were primarily paramagnetic polarons. As the doping time increased, the EPR intensity gradually decreased to zero, confirming the transition from polarons to spinless bipolarons.^{36,37} Notably, the EPR signal of P(Py2FT) was still observable after 5 min of TDAE doping, whereas the EPR signal of P(PyT) almost disappeared, suggesting that polarons in P(PyT) can transition to bipolarons at a relatively lower doping level ([Supporting Information Figure S15](#)).

Time-dependent density functional theory (TD-DFT) calculations were employed to simulate the absorption spectra, which agree well with the experimental results ([Supporting Information Figures S12–S14](#)). At low doping levels, polarons dominated, exhibiting a characteristic absorption around 2000 nm. At high doping levels, polarons combined to form doubly charged bipolarons, resulting in enhanced bipolaron absorption below 1000 nm and a decrease in the intensity of polaron peaks. Interestingly, our calculations demonstrated that these bipolarons delocalized across neighboring polymer chains, which differs from the typical observation where bipolarons originate within the same chain.^{35,38} The formation of bipolarons can be attributed to many factors, such as polymer interchain coupling,³⁹ dopant/counterion effects,^{40,41} and polymer structures.³⁵ In this system, we assumed that these sidechain-free cationic polymers exhibited tight molecular packings, facilitating the formation of interchain bipolarons, similar to what has been observed in poly(3,4-ethylenedioxythiophene) polystyrene sulfonate (PEDOT:PSS).⁴²

This assumption was further confirmed by GIWAXS measurements (Figure 4a,b and [Supporting Information Figure S16](#)). The cell parameters are summarized in [Supporting Information Table S2](#). Both cationic polymers exhibited notably small lamellar stacking distances, measuring 9.35 Å for P(Py2FT) and 8.36 Å for P(PyT). Despite conventional wisdom that suggests charge repulsion between ionic species,⁴³ we observed that the π - π stacking distances of these cationic polymers were below 3.6 Å, similar to those observed in conventional conjugated polymers.^{44–46} However, there are still differences between the two cationic polymers: The P(PyT) sample shows a predominantly face-on texture, as is evident from the lack of a pronounced in-plane π - π stacking peak. In contrast, the obvious π - π diffraction peaks in both the in-plane and out-of-plane directions suggest a coexistence of face-on and edge-on crystallites in P(Py2FT) (Figure 4a,b). This mixed orientation promoted the formation of three-dimensional (3D) conduction channels for more effective charge transport in P(Py2FT) (Figure 4c),^{17,47,48} potentially affecting its charge-carrier mobility after doping. After TDAE doping for 30 min, P(Py2FT) exhibited a three-fold increase in carrier concentration and simultaneously a five-fold increase in conductivity compared to P(PyT), indicating a 1.6 times higher mobility for P(Py2FT). Additionally, we noted a reduction in the π - π stacking distance from 3.59 Å (P(PyT)) to 3.51 Å (P(Py2FT)), which is consistent with the improved backbone planarity of P(Py2FT). Typically, the introduction of dopants tends to distort molecular conformations and disrupt molecular packing, resulting in expanded stacking distances and increased paracrystalline disorder.^{32,49,50} Interestingly, doped P(Py2FT) exhibited a simultaneous decrease in both π - π stacking and lamellar distances (Figure 4a,b and [Supporting Information Figure S17](#)). Additionally, the paracrystallinity parameter $g_{\pi-\pi}$ dropped with respect to undoped P(Py2FT), indicating a reduction in structural disorder. These findings suggest enhanced backbone planarity and improved molecular packing order within P(Py2FT) after molecular doping.

The discovery of doping-enhanced backbone planarity has triggered our great interest. Previous studies mainly focused on designing planar polymer backbones in neutral states.^{51,52} However, many applications, such as OTEs, need heavily-doped materials for effective operation. Therefore, more efforts should be devoted to molecular designs that consider polymer properties in doped states. To elucidate how doping improves backbone planarity, we performed relaxed PES calculations for dimers of cationic polymers in doped states (Figure 4d). Compared to neutral states, the predominant conformations of doped (Py2FT)₂ exhibited a torsion angle around 0°, with the barrier height increasing by 6.11 kcal mol⁻¹. However, (PyT)₂ displayed a flatter torsion potential around the minimum and less increase

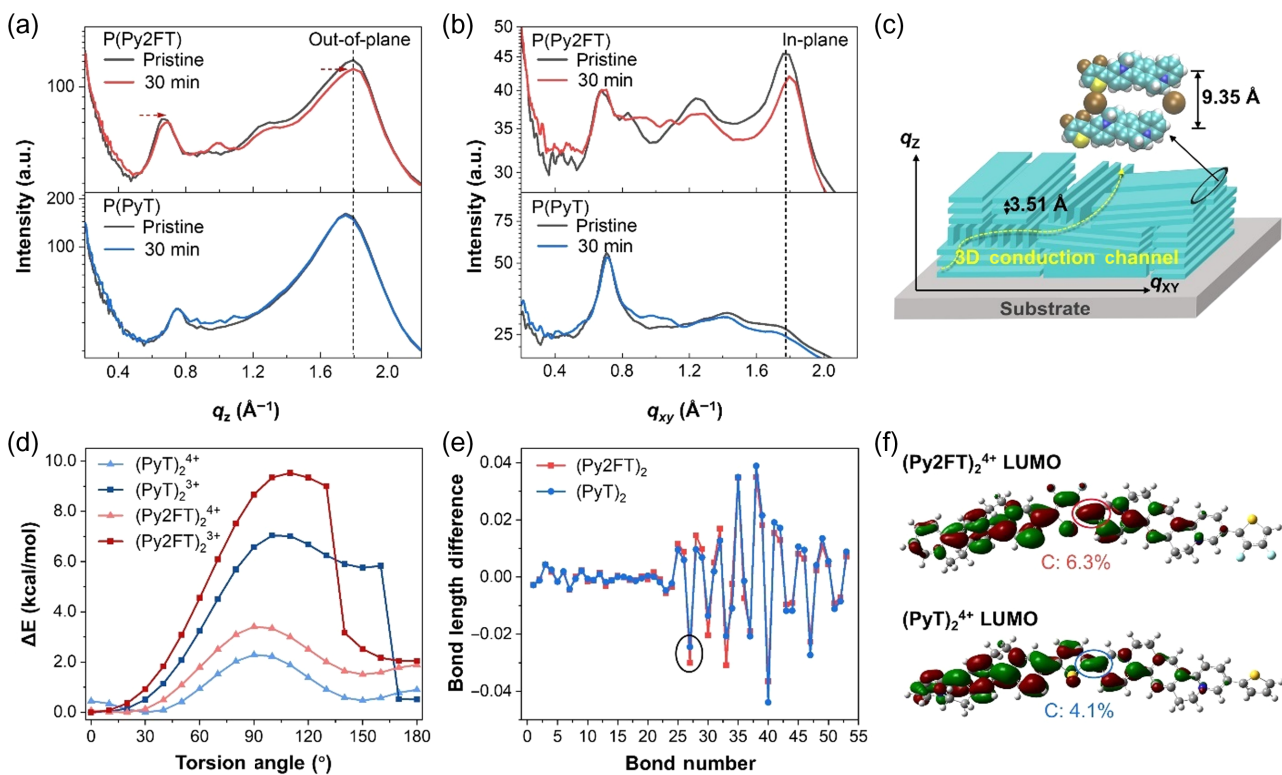


Figure 4 | (a) Out-of-plane and (b) in-plane 1D scattering intensity plots of pristine and doped polymer films, measured by GIWAXS. (c) Schematic illustration of the 3D conduction channel. (d) Relaxed PES of dimers in undoped states $[(\text{Py2FT})_2]^{4+}$ and $[(\text{PyT})_2]^{4+}$ and doped states $[(\text{Py2FT})_2]^{3+}$ and $[(\text{PyT})_2]^{3+}$. (e) Bond length analysis (BLA) of $(\text{Py2FT})_2$ and $(\text{PyT})_2$. The bond length difference refers to the variation in bond length between the undoped and doped states of dimers. Specifically, the C-C bonds connecting the cationic building blocks and thiophenes are highlighted with dark circles. (f) Molecular orbital wavefunctions of the LUMO bands for undoped dimers. The indicated percentages denote the contribution from the C-C linkages between the thiophene and the cationic building block to the LUMO, according to the natural atomic orbital population analysis.

in the barrier height after doping. Since the backbone planarity is particularly sensitive to the length of chemical bonds, we analyzed the difference in bond lengths between neutral and doped polymer dimers. The convention used for the bond numbering is indicated in Supporting Information Figure S21, and the C-C bond that links the repeating units is highlighted with a dark circle in Figure 4e. After *n*-doping, the C-C linkage significantly shortened for both cationic polymers, indicating an increased double-bond character. Specifically, the C-C linkage of $(\text{Py2FT})_2$ decreased by 0.030\AA , which is larger than that for $\text{P}(\text{PyT})_2$ (0.024\AA). The doping-enhanced backbone planarity of both polymers can be attributed to the composition of their frontier molecular orbitals. Compared to $(\text{PyT})_2^{4+}$, the fluorine substituents within $(\text{Py2FT})_2^{4+}$ stabilize the LUMO, resulting in a larger contribution from the C-C linkage to the LUMO: 6.3% for $(\text{Py2FT})_2^{4+}$ and 4.1% for $(\text{PyT})_2^{4+}$ (Figure 4f). In the singly occupied molecular orbital split from LUMO upon doping, we observed the consistently larger contribution from the C-C linkage of $\text{P}(\text{Py2FT})$ compared to $\text{P}(\text{PyT})$.

(Supporting Information Figure S22). This increased electron density along the C-C linkage led to a more pronounced enhancement in bond strength after doping, thus resulting in higher backbone planarity. We extended our analysis to investigate the backbone planarity of other advanced conjugated polymers in doped states (Supporting Information Figures S23 and S24). Among conventional *n*-type conjugated polymers, the contribution of the C-C linkage to LUMO generally remains below 4.1%, with only a slight improvement in backbone planarity after doping. These results indicate that introducing cationic building blocks is an effective method to improve the backbone planarity of *n*-type conjugated polymers at doped states.

Conclusion

In summary, we have designed and synthesized a water/alcohol processable *n*-type conjugated polymer, $\text{P}(\text{Py2FT})$. Compared to its reference polymer, $\text{P}(\text{Py2FT})$ displays a lower LUMO level, higher doping efficiency,

enhanced backbone planarity, and better molecular packing. With P(Py2FT), we have achieved a higher *n*-type electrical conductivity of up to 28.1 S cm^{-1} and a maximum thermoelectric PF of $28.7 \mu\text{W m}^{-1} \text{ K}^{-2}$, comparable to some conventional *n*-type conjugated polymers reported recently. Furthermore, our study has demonstrated that the introduction of cationic building blocks can bring about tight polymer packing and enhanced backbone planarity, especially under heavily doped states. Our research not only provides a new molecular design guideline for enhancing the performance of cationic conjugated polymers, but it also presents a viable approach to tackle the sidechain challenges in traditional conjugated polymers. We anticipate that our findings will encourage more researchers to devote their efforts to sidechain-free cationic polymers, ultimately elevating their performance to rival or even surpass that of traditional conjugated polymers.

Supporting Information

Supporting Information is available and includes device fabrication details; GPC, TGA, and CV traces; UV-vis-NIR spectra; XPS data; GIWAXS images and analysis; DFT calculations; and monomer and polymer synthesis and characterization.

Conflict of Interest

There is no conflict of interest to report.

Acknowledgments

This work is supported financially by the National Key R&D Program of China (grant no. 2022YFE0130600), the National Natural Science Foundation of China (grant nos. 22075001 and 92156019), and the King Abdullah University of Science and Technology (KAUST) Competitive Research Grants under award no. ORA-CRG10-2021-4668. X.G. and Y.W. gratefully acknowledge support from the KAUST Office of Sponsored Research under award no. OSA-CRG2021-4668. The computational part of this work is supported by the High-performance Computing Platform of Peking University. We gratefully acknowledge the Molecular Materials and Nanofabrication Laboratory in the College of Chemistry, Electron Microscopy Laboratory, and Materials Processing and Analysis Center of Peking University for the use of their instruments.

References

1. Russ, B.; Glaudell, A.; Urban, J. J.; Chabiny, M. L.; Segalman, R. A. Organic Thermoelectric Materials for Energy Harvesting and Temperature Control. *Nat. Rev. Mater.* **2016**, *1*, 16050.
2. Kim, G. H.; Shao, L.; Zhang, K.; Pipe, K. P. Engineered Doping of Organic Semiconductors for Enhanced Thermoelectric Efficiency. *Nat. Mater.* **2013**, *12*, 719–723.
3. Bubnova, O.; Khan, Z. U.; Malti, A.; Braun, S.; Fahlman, M.; Berggren, M.; Crispin, X. Optimization of the Thermoelectric Figure of Merit in the Conducting Polymer Poly(3,4-Ethylene-nedioxythiophene). *Nat. Mater.* **2011**, *10*, 429–433.
4. Patel Shreyesh, N.; Glaudell Anne, M.; Peterson Kelly, A.; Thomas Elayne, M.; O'Hara Kathryn, A.; Lim, E.; Chabiny Michael, L. Morphology Controls the Thermoelectric Power Factor of a Doped Semiconducting Polymer. *Sci. Adv.* **2017**, *3*, e1700434.
5. Wang, S.; Sun, H.; Ail, U.; Vagin, M.; Persson, P. O.; Andreasen, J. W.; Thiel, W.; Berggren, M.; Crispin, X.; Fazzi, D. J. A. M. Thermoelectric Properties of Solution-Processed N-Doped Ladder-Type Conducting Polymers. *Adv. Mater.* **2016**, *28*, 10764–10771.
6. Yu, Z.-D.; Lu, Y.; Wang, Z.-Y.; Un, H.-I.; Zelewski, S. J.; Cui, Y.; You, H.-Y.; Liu, Y.; Xie, K.-F.; Yao, Z.-F.; He, Y.-C.; Wang, J.-Y.; Hu, W.-B.; Sirringhaus, H.; Pei, J. High N-Type and P-Type Conductivities and Power Factors Achieved in a Single Conjugated Polymer. *Sci. Adv.* **2023**, *9*, eadf3495.
7. Feng, K.; Guo, H.; Wang, J.; Shi, Y.; Wu, Z.; Su, M.; Zhang, X.; Son, J. H.; Woo, H. Y.; Guo, X. Cyano-Functionalized Bithiophene Imide-Based N-Type Polymer Semiconductors: Synthesis, Structure–Property Correlations, and Thermoelectric Performance. *J. Am. Chem. Soc.* **2021**, *143*, 1539–1552.
8. Yan, H.; Chen, Z.; Zheng, Y.; Newman, C.; Quinn, J. R.; Dötz, F.; Kastler, M.; Facchetti, A. A High-Mobility Electron-Transporting Polymer for Printed Transistors. *Nature* **2009**, *457*, 679–686.
9. Li, Y.; Singh, S. P.; Sonar, P. A High Mobility P-Type DPP-Thieno[3,2-B]Thiophene Copolymer for Organic Thin-Film Transistors. *Adv. Mater.* **2010**, *22*, 4862–4866.
10. Wang, E.; Ma, Z.; Zhang, Z.; Vandewal, K.; Henriksson, P.; Inganäs, O.; Zhang, F.; Andersson, M. R. An Easily Accessible Isoindigo-Based Polymer for High-Performance Polymer Solar Cells. *J. Am. Chem. Soc.* **2011**, *133*, 14244–14247.
11. Lei, T.; Dou, J.-H.; Cao, X.-Y.; Wang, J.-Y.; Pei, J. A BDOPV-Based Donor-Acceptor Polymer for High-Performance N-Type and Oxygen-Doped Ambipolar Field-Effect Transistors. *Adv. Mater.* **2013**, *25*, 6589–6593.
12. Huang, H.; Chen, Z.; Ortiz, R. P.; Newman, C.; Usta, H.; Lou, S.; Youn, J.; Noh, Y.-Y.; Baeg, K.-J.; Chen, L. X.; Facchetti, A.; Marks, T. Combining Electron-Neutral Building Blocks with Intramolecular “Conformational Locks” Affords Stable, High-Mobility P- and N-Channel Polymer Semiconductors. *J. Am. Chem. Soc.* **2012**, *134*, 10966–10973.
13. Huang, H.; Yang, L.; Facchetti, A.; Marks, T. J. Organic and Polymeric Semiconductors Enhanced by Noncovalent Conformational Locks. *Chem. Rev.* **2017**, *117*, 10291–10318.
14. Chen, H.; Moser, M.; Wang, S.; Jellett, C.; Thorley, K.; Harrison, G. T.; Jiao, X.; Xiao, M.; Purushothaman, B.; Alsufyani, M.; Bristow, H.; De Wolf, S.; Gasparini, N.; Wadsworth, A.; McNeill, C. R.; Sirringhaus, H.; Fabiano, S.; McCulloch, I. Acene Ring Size Optimization in Fused Lactam

- Polymers Enabling High N-Type Organic Thermoelectric Performance. *J. Am. Chem. Soc.* **2021**, *143*, 260–268.
15. Xiao, M.; Carey, R. L.; Chen, H.; Jiao, X.; Lemaur, V.; Schott, S.; Nikolka, M.; Jellett, C.; Sadhanala, A.; Rogers, S.; Senanayak, S. P.; Onwubiko, A.; Han, S.; Zhang, Z.; Abdijalebi, M.; Zhang, Y.; Thomas, T. H.; Mahmoudi, N.; Lai, L.; Selezneva, E.; Ren, X.; Nguyen, M.; Wang, Q.; Jacobs, I.; Yue, W.; McNeill, C. R.; Liu, G.; Beljonne, D.; McCulloch, I.; Sirringhaus, H. Charge Transport Physics of a Unique Class of Rigid-Rod Conjugated Polymers with Fused-Ring Conjugated Units Linked by Double Carbon-Carbon Bonds. *Sci. Adv.* **2021**, *7*, eabe5280.
16. Danielsen, S. P. O.; Bridges, C. R.; Segalman, R. A. Chain Stiffness of Donor-Acceptor Conjugated Polymers in Solution. *Macromolecules* **2022**, *55*, 437–449.
17. Mei, J.; Kim, D. H.; Ayzner, A. L.; Toney, M. F.; Bao, Z. Siloxane-Terminated Solubilizing Side Chains: Bringing Conjugated Polymer Backbones Closer and Boosting Hole Mobilities in Thin-Film Transistors. *J. Am. Chem. Soc.* **2011**, *133*, 20130–20133.
18. Lei, T.; Dou, J.-H.; Pei, J. Influence of Alkyl Chain Branching Positions on the Hole Mobilities of Polymer Thin-Film Transistors. *Adv. Mater.* **2012**, *24*, 6457–6461.
19. Meager, I.; Ashraf, R. S.; Mollinger, S.; Schroeder, B. C.; Bronstein, H.; Beatrup, D.; Vezie, M. S.; Kirchartz, T.; Salleo, A.; Nelson, J.; McCulloch, I. Photocurrent Enhancement from Diketopyrrolopyrrole Polymer Solar Cells through Alkyl-Chain Branching Point Manipulation. *J. Am. Chem. Soc.* **2013**, *135*, 11537–11540.
20. Ke, Z.; Abtahi, A.; Hwang, J.; Chen, K.; Chaudhary, J.; Song, I.; Perera, K.; You, L.; Baustert, K. N.; Graham, K. R.; Mei, J. Highly Conductive and Solution-Processable N-Doped Transparent Organic Conductor. *J. Am. Chem. Soc.* **2023**, *145*, 3706–3715.
21. Tang, H.; Liang, Y.; Liu, C.; Hu, Z.; Deng, Y.; Guo, H.; Yu, Z.; Song, A.; Zhao, H.; Zhao, D.; Zhang, Y.; Guo, X.; Pei, J.; Ma, Y.; Cao, Y.; Huang, F. A Solution-Processed N-Type Conducting Polymer with Ultrahigh Conductivity. *Nature* **2022**, *611*, 271–277.
22. Frisch, M. J.; Trucks, G. W.; Schlegel, H. B.; Scuseria, G. E.; Robb, M. A.; Cheeseman, J. R.; Scalmani, G.; Barone, V.; Petersson, G. A.; Nakatsuji, H.; Li, X.; Caricato, M.; Marenich, A. V.; Bloino, J.; Janesko, B. G.; Gomperts, R.; Mennucci, B.; Hratchian, H. P.; Ortiz, J. V.; Izmaylov, A. F.; Sonnenberg, J. L.; Williams-Young, D.; Ding, F.; Lipparini, F.; Egidi, F.; Goings, J.; Peng, B.; Petrone, A.; Henderson, T.; Ranasinghe, D.; Zakrzewski, V. G.; Gao, J.; Rega, N.; Zheng, G.; Liang, W.; Hada, M.; Ehara, M.; Toyota, K.; Fukuda, R.; Hasegawa, J.; Ishida, M.; Nakajima, T.; Honda, Y.; Kitao, O.; Nakai, H.; Vreven, T.; Throssell, K.; Montgomery, J. A. Jr.; Peralta, J. E.; Ogliaro, F.; Bearpark, M. J.; Heyd, J. J.; Brothers, E. N.; Kudin, K. N.; Staroverov, V. N.; Keith, T. A.; Kobayashi, R.; Normand, J.; Raghavachari, K.; Rendell, A. P.; Burant, J. C.; Iyengar, S. S.; Tomasi, J.; Cossi, M.; Millam, J. M.; Klene, M.; Adamo, C.; Cammi, R.; Ochterski, J. W.; Martin, R. L.; Morokuma, K.; Farkas, O.; Foresman, J. B.; Fox, D. J. *Gaussian 16, Revision C.01*; Gaussian, Inc.: Wallingford, CT, **2016**.
23. Huang, Z.; Li, P.; Lei, Y.; Deng, X.-Y.; Chen, Y.-N.; Tian, S.; Pan, X.; Lei, X.; Song, C.; Zheng, Y.; Wang, J.-Y.; Zhang, Z.; Lei, T. Azonia-Naphthalene: A Cationic Hydrophilic Building Block for Stable N-Type Organic Mixed Ionic-Electronic Conductors. *Angew. Chem. Int. Ed.* **2024**, *63*, e202313260.
24. Izuohara, D.; Swager, T. M. Poly(Pyridinium Phenylene)s: Water-Soluble N-Type Polymers. *J. Am. Chem. Soc.* **2009**, *131*, 17724–17725.
25. Rochat, S.; Swager, T. M. Fluorescence Sensing of Amine Vapors Using a Cationic Conjugated Polymer Combined with Various Anions. *Angew. Chem. Int. Ed.* **2014**, *53*, 9792–9796.
26. Huang, D.; Yao, H.; Cui, Y.; Zou, Y.; Zhang, F.; Wang, C.; Shen, H.; Jin, W.; Zhu, J.; Diao, Y. Conjugated-Backbone Effect of Organic Small Molecules for N-Type Thermoelectric Materials with ZT over 0.2. *J. Am. Chem. Soc.* **2017**, *139*, 13013–13023.
27. Jackson, N. E.; Savoie, B. M.; Kohlstedt, K. L.; Olvera de la Cruz, M.; Schatz, G. C.; Chen, L. X.; Ratner, M. A. Controlling Conformations of Conjugated Polymers and Small Molecules: The Role of Nonbonding Interactions. *J. Am. Chem. Soc.* **2013**, *135*, 10475–10483.
28. Ehrenreich, P.; Birkhold, S. T.; Zimmermann, E.; Hu, H.; Kim, K.-D.; Weickert, J.; Pfadler, T.; Schmidt-Mende, L. H. Aggregate Analysis of P3HT Thin Films—Capability and Limitation of Photoluminescence and UV/Vis Spectroscopy. *Sci. Rep.* **2016**, *6*, 32434.
29. Yang, C.-Y.; Jin, W.-L.; Wang, J.; Ding, Y.-F.; Nong, S.; Shi, K.; Lu, Y.; Dai, Y.-Z.; Zhuang, F.-D.; Lei, T.; Di, C.-A.; Zhu, D.; Wang, J.-Y.; Pei, J. Enhancing the N-Type Conductivity and Thermoelectric Performance of Donor-Acceptor Copolymers through Donor Engineering. *Adv. Mater.* **2018**, *30*, 1802850.
30. Yan, X.; Xiong, M.; Li, J.-T.; Zhang, S.; Ahmad, Z.; Lu, Y.; Wang, Z.-Y.; Yao, Z.-F.; Wang, J.-Y.; Gu, X.; Lei, T. Pyrazine-Flanked Diketopyrrolopyrrole (DPP): A New Polymer Building Block for High-Performance N-Type Organic Thermoelectrics. *J. Am. Chem. Soc.* **2019**, *141*, 20215–20221.
31. Burkholder, C.; Dolbier, W. R.; Médebielle, M. Reaction of the 2-(Bromodifluoromethyl)Benzoxazole with Tetrakis (Dimethylamino)Ethylene (TDAE) in the Presence of Aldehydes. A Convenient Synthesis of 2-(Difluoromethyl)Benzoxazole Alcohols. *Tetrahedron Lett.* **1997**, *38*, 821–824.
32. Yang, C.-Y.; Ding, Y.-F.; Huang, D.; Wang, J.; Yao, Z.-F.; Huang, C.-X.; Lu, Y.; Un, H.-I.; Zhuang, F.-D.; Dou, J.-H.; Di, C.-A.; Zhu, D.; Wang, J.-Y.; Lei, T.; Pei, J. A Thermally Activated and Highly Miscible Dopant for N-Type Organic Thermoelectrics. *Nat. Commun.* **2020**, *11*, 3292.
33. Boyle, C. J.; Upadhyaya, M.; Wang, P.; Renna, L. A.; Lu-Díaz, M.; Pyo Jeong, S.; Hight-Huf, N.; Korugic-Karasz, L.; Barnes, M. D.; Aksamija, Z.; Venkataraman, D. Tuning Charge Transport Dynamics Via Clustering of Doping in Organic Semiconductor Thin Films. *Nat. Commun.* **2019**, *10*, 2827.
34. Tu, L.; Wang, J.; Wu, Z.; Li, J.; Yang, W.; Liu, B.; Wu, S.; Xia, X.; Wang, Y.; Woo, H. Y.; Shi, Y. Cyano-Functionalized Pyrazine: A Structurally Simple and Easily Accessible Electron-Deficient Building Block for N-Type Organic

- Thermoelectric Polymers. *Angew. Chem. Int. Ed.* **2024**, *63*, e202319658.
35. Voss, M. G.; Challa, J. R.; Scholes, D. T.; Yee, P. Y.; Wu, E. C.; Liu, X.; Park, S. J.; León Ruiz, O.; Subramaniyan, S.; Chen, M.; Jenekhe, S. A.; Wang, X.; Tolbert, S. H.; Schwartz, B. J. Driving Force and Optical Signatures of Bipolaron Formation in Chemically Doped Conjugated Polymers. *Adv. Mater.* **2021**, *33*, 2000228.
36. Barlow, S.; Risko, C.; Chung, S.-J.; Tucker, N. M.; Coropceanu, V.; Jones, S. C.; Levi, Z.; Brédas, J.-L.; Marder, S. R. Intervalence Transitions in the Mixed-Valence Monocations of Bis(Triarylamines) Linked with Vinylene and Phenylene-Vinylene Bridges. *J. Am. Chem. Soc.* **2005**, *127*, 16900-16911.
37. van Haare, J. A. E. H.; Havinga, E. E.; van Dongen, J. L. J.; Janssen, R. A. J.; Cornil, J.; Brédas, J.-L. Redox States of Long Oligothiophenes: Two Polarons on a Single Chain. *Chem. Eur. J.* **1998**, *4*, 1509-1522.
38. Bakalis, J.; Cook, A. R.; Asaoka, S.; Forster, M.; Scherf, U.; Miller, J. R. Polarons, Compressed Polarons, and Bipolarons in Conjugated Polymers. *J. Phys. Chem. C* **2014**, *118*, 114-125.
39. Di, B.; Meng, Y.; Wang, Y. D.; Liu, X. J.; An, Z. Formation and Evolution Dynamics of Bipolarons in Conjugated Polymers. *J. Phys. Chem. B* **2011**, *115*, 964-971.
40. Warren, R.; Cho, E.; Li, H.; Bredas, J.-L.; Koch, N. Understanding the Double Doping of Organic Semiconductors via State Energy Renormalization Upon Charging. *ACS Mater. Lett.* **2022**, *4*, 2051-2057.
41. Zaikowski, L.; Kaur, P.; Gelfond, C.; Selvaggio, E.; Asaoka, S.; Wu, Q.; Chen, H.-C.; Takeda, N.; Cook, A. R.; Yang, A.; Rosanelli, J.; Miller, J. R. Polarons, Bipolarons, and Side-by-Side Polarons in Reduction of Oligofluorenes. *J. Am. Chem. Soc.* **2012**, *134*, 10852-10863.
42. Apperloo, J. J.; Groenendaal, L. B.; Verheyen, H.; Jayakannan, M.; Janssen, R. A. J.; Dkhissi, A.; Beljonne, D.; Lazzaroni, R.; Brédas, J.-L. Optical and Redox Properties of a Series of 3,4-Ethylenedioxythiophene Oligomers. *Chem. Eur. J.* **2002**, *8*, 2384-2396.
43. Li, X.; Xu, H.-S.; Leng, K.; Chee, S. W.; Zhao, X.; Jain, N.; Xu, H.; Qiao, J.; Gao, Q.; Park, I.-H.; Quek, S. Y.; Mirsaidov, U.; Loh, K. P. Partitioning the Interlayer Space of Covalent Organic Frameworks by Embedding Pseudorotaxanes in Their Backbones. *Nat. Chem.* **2020**, *12*, 1115-1122.
44. Yan, X.; Xiong, M.; Deng, X.-Y.; Liu, K.-K.; Li, J.-T.; Wang, X.-Q.; Zhang, S.; Prine, N.; Zhang, Z.; Huang, W.; Wang, Y.; Wang, J.-Y.; Gu, X.; So, S. K.; Zhu, J.; Lei, T. Approaching Disorder-Tolerant Semiconducting Polymers. *Nat. Commun.* **2021**, *12*, 5723.
45. Lu, Y.; Yu, Z.-D.; Zhang, R.-Z.; Yao, Z.-F.; You, H.-Y.; Jiang, L.; Un, H.-I.; Dong, B.-W.; Xiong, M.; Wang, J.-Y.; Pei, J. Rigid Coplanar Polymers for Stable N-Type Polymer Thermoelectrics. *Angew. Chem. Int. Ed.* **2019**, *58*, 11390-11394.
46. Venkateshvaran, D.; Nikolka, M.; Sadhanala, A.; Lemaur, V.; Zelazny, M.; Kepa, M.; Hurhangee, M.; Kronemeijer, A. J.; Pecunia, V.; Nasrallah, I.; Romanov, I.; Broch, K.; McCulloch, I.; Emin, D.; Olivier, Y.; Cornil, J.; Beljonne, D.; Sirringhaus, H. Approaching Disorder-Free Transport in High-Mobility Conjugated Polymers. *Nature* **2014**, *515*, 384-388.
47. Rivnay, J.; Steyrleuthner, R.; Jimison, L. H.; Casadei, A.; Chen, Z.; Toney, M. F.; Facchetti, A.; Neher, D.; Salleo, A. Drastic Control of Texture in a High Performance N-Type Polymeric Semiconductor and Implications for Charge Transport. *Macromolecules* **2011**, *44*, 5246-5255.
48. Zhang, X.; Richter, L. J.; DeLongchamp, D. M.; Kline, R. J.; Hammond, M. R.; McCulloch, I.; Heeney, M.; Ashraf, R. S.; Smith, J. N.; Anthopoulos, T. D.; Schroeder, B.; Geerts, Y. H.; Fischer, D. A.; Toney, M. F. Molecular Packing of High-Mobility Diketo Pyrrolo-Pyrrole Polymer Semiconductors with Branched Alkyl Side Chains. *J. Am. Chem. Soc.* **2011**, *133*, 15073-15084.
49. Lu, Y.; Yu, Z.-D.; Liu, Y.; Ding, Y.-F.; Yang, C.-Y.; Yao, Z.-F.; Wang, Z.-Y.; You, H.-Y.; Cheng, X.-F.; Tang, B.; Wang, J.-Y.; Pei, J. The Critical Role of Dopant Cations in Electrical Conductivity and Thermoelectric Performance of N-Doped Polymers. *J. Am. Chem. Soc.* **2020**, *142*, 15340-15348.
50. Jacobs, I. E.; D'Avino, G.; Lemaur, V.; Lin, Y.; Huang, Y.; Chen, C.; Harrelson, T. F.; Wood, W.; Spalek, L. J.; Mustafa, T.; O'Keefe, C. A.; Ren, X.; Simatos, D.; Tjhe, D.; Statz, M.; Strzalka, J. W.; Lee, J.-K.; McCulloch, I.; Fratini, S.; Beljonne, D.; Sirringhaus, H. Structural and Dynamic Disorder, Not Ionic Trapping, Controls Charge Transport in Highly Doped Conducting Polymers. *J. Am. Chem. Soc.* **2022**, *144*, 3005-3019.
51. Bronstein, H.; Nielsen, C. B.; Schroeder, B. C.; McCulloch, I. The Role of Chemical Design in the Performance of Organic Semiconductors. *Nat. Rev. Chem.* **2020**, *4*, 66-77.
52. Fratini, S.; Nikolka, M.; Salleo, A.; Schweicher, G.; Sirringhaus, H. Charge Transport in High-Mobility Conjugated Polymers and Molecular Semiconductors. *Nat. Mater.* **2020**, *19*, 491-502.